Agricultural and Forest Meteorology xxx (xxxx) xxx–xxx

Contents lists available at ScienceDirect

Agricultural and Forest Meteorology

journal homepage: www.elsevier.com/locate/agrformet

Investigating the mechanisms responsible for the lack of surface energy balance closure in a central Amazonian tropical rainforest

Tobias Gerken[a,b,*], Benjamin L. Ruddell[c], Jose D. Fuentes[b], Alessandro Araújo[d], Nathaniel A. Brunsell[e], Jair Maia[f], Antonio Manzi[g], Juliane Mercer[a], Rosa Nascimento dos Santos[f], Celso von Randow[h], Paul C. Stoy[a]

[a] Department of Land Resources and Environmental Sciences, Montana State University, MT, USA
[b] Department of Meteorology and Atmospheric Science, The Pennsylvania State University, University Park, PA, USA
[c] School of Informatics, Computing, and Cyber Systems, Northern Arizona University, AZ, USA
[d] Embrapa Amazônia Oriental, Belém, PA, Brazil
[e] Department of Geography and Atmospheric Science, University of Kansas, KS, USA
[f] Universidade do Estado do Amazonas (UEA), Manaus, AM, Brazil
[g] Instituto Nacional de Pesquisas da Amazônia (INPA), Manaus, AM, Brazil
[h] National Institute for Space Research(INPE), São José dos Campos, SP, Brazil

ARTICLE INFO

Keywords:
Eddy covariance
Information flow
Latent heat flux
Sensible heat flux
Tropical rainforest

ABSTRACT

This work investigates the diurnal and seasonal behavior of the energy balance residual (*E*) that results from the observed difference between available energy and the turbulent fluxes of sensible heat (*H*) and latent heat (*LE*) at the FLUXNET BR-Ma2 site located in the Brazilian central Amazon rainforest. The behavior of *E* is analyzed by extending the eddy covariance averaging length from 30 min to 4 h and by applying an Information Flow Dynamical Process Network to diagnose processes and conditions affecting *E* across different seasons. Results show that the seasonal turbulent flux dynamics and the Bowen ratio are primarily driven by net radiation (R_n), with substantial sub-seasonal variability. The Bowen ratio increased from 0.25 in April to 0.4 at the end of September. Extension of the averaging length from 0.5 (94.6% closure) to 4 h and thus inclusion of longer timescale eddies and mesoscale processes closes the energy balance and lead to an increase in the Bowen ratio, thus highlighting the importance of additional *H* to E. Information flow analysis reveals that the components of the energy balance explain between 25 and 40% of the total Shannon entropy with higher values during the wet season than the dry season. Dry season information flow from the buoyancy flux to *E* are 30–50% larger than that from *H*, indicating the potential importance of buoyancy fluxes to closing *E*. While the low closure highlights additional sources not captured in the flux data and random measurement errors contributing to *E*, the findings of the information flow and averaging length analysis are consistent with the impact of mesoscale circulations, which tend to transport more *H* than *LE*, on the lack of closure.

1. Introduction

Eddy covariance has quickly become the global standard for estimating the exchange of water, heat, and trace gases between ecosystems and the atmosphere (Baldocchi, 2014, 2008; Baldocchi et al., 2001). Despite its promise as a largely non-invasive technology for the near-continuous estimates of surface-atmosphere matter and energy fluxes, most eddy covariance measurements do not fully close the energy balance (Franssen et al., 2010; Stoy et al., 2013; Wilson et al., 2002). After decades of research in developing the fundamental equations for eddy covariance, developing instruments, describing corrections, and characterizing measurement uncertainty (e.g. Gu et al., 2012; Leuning et al., 2012; Massman and Clement, 2004; Massman and Lee, 2002; Moncrieff et al., 2005; Richardson et al., 2006), fewer than half of the sites in global databases can report energy balance closure on a diurnal basis (Leuning et al., 2012). It is critical to understand what causes the lack of energy balance closure (*E*, often called the energy balance residual) to improve the instrumentation and theory that underlie the eddy covariance technique in order to gain a better understanding of the role of surface-atmosphere exchange in the Earth system.

Investigations into the mechanisms responsible for *E* are ongoing.

* Corresponding author at: Department of Land Resources and Environmental Sciences, Montana State University, Bozeman, Montana 59717, USA.
E-mail address: tobias.gerken@montana.edu (T. Gerken).

http://dx.doi.org/10.1016/j.agrformet.2017.03.023
Received 1 January 2017; Received in revised form 12 March 2017; Accepted 29 March 2017

Careful critiques of sonic anemometry reveal that non-orthogonal transducer placement may be responsible for up to 15% of the discrepancy of sensible heat fluxes (*H*) (Frank et al., 2013; Kochendorfer et al., 2012). Other studies argue that mesoscale meteorological motions that are not measured using conventional sonic anemometry, and/or vary at characteristic timescales longer than the conventional half-hour averaging period, are primarily responsible for *E* (Foken, 2008; Foken et al., 2011; Mauder et al., 2010, 2007; Panin and Bernhofer, 2008). An extension of this line of reasoning is that *E* may scale with the buoyancy flux (*HB*) (Charuchittipan et al., 2014). Both lines of evidence suggest that *H* may dominate *E* such that corrections based on the Bowen ratio (β) (Twine et al., 2000) may not be accurate, depending on how mismeasurement of the vertical variance of wind velocity (*w'*) impacts *H versus* latent heat flux (*LE*). At the same time, mismatches between the measurement footprints of net radiation (R_n) and turbulent fluxes, whose footprint is highly variable with atmospheric stability, may be responsible for *E* at individual sites.

Acknowledging the critical roles of improvements to instrumentation and our knowledge of atmospheric boundary-layer processes, it is necessary to quantify − to the best of our ability − the causes of *E* on a site-by-site basis. Thousands of site-years of eddy covariance data exist (Baldocchi, 2008; Stoy et al., 2009), and careful interpretation of these data are required to understand trends of surface-atmosphere exchange on a changing planet (Jung et al., 2010). We argue that querying existing data to uncover the 'symptoms' of *E* using a data-driven approach can provide information to help further refine the eddy covariance technique.

Here, we study *E* using eddy covariance measurements from a rainforest in the central Brazilian Amazon (Site code: BR-Ma2). We combine a critical analysis of the eddy covariance averaging period with a novel information theory-based interpretation of information flows amongst energy balance terms. The latter analysis asks, in effect, how much information from energy flux time series is transferred to *E* (Ruddell et al., 2013). Previous research at BR-Ma2 demonstrated that the energy balance was approximately closed at longer averaging periods (Malhi et al., 2002), but did not interpret the terms responsible for *E*. Likewise, previous investigations using information networks revealed bi-directional links between surface and atmospheric processes and quantified their seasonal dynamics and states (Ruddell et al., 2015; Ruddell and Kumar, 2009a,b), but has not been used to quantify how information from different flux terms contributes to *E* from forested ecosystems to date.

We focus our investigation on a tropical forest for a number of reasons. Tropical forests help regulate the amount of heat and moisture that enters the atmosphere and is available for deep convection and thereby contribute to regional and global heat transport (Avissar and Werth, 2005). Tropical ecosystems are also amongst the Earth's most threatened (Kim et al., 2015), with consequences not only for biodiversity, but also for global climate services such as carbon assimilation and water resources (e.g. Medvigy et al., 2013). Land surface models are in the nascent stages of recognizing the functional diversity of tropical forests (Pavlick et al., 2013), and recent approaches that incorporate species-specific hydrology demonstrate that they may be more resilient to hydrologic and climate disturbances (Levine et al., 2016) than previously assumed (Cox et al., 2000).

At the same time, global syntheses indicate that tropical forests are amongst the most isohydric of any terrestrial ecosystem (Fisher et al., 2006; Konings and Gentine, 2016), suggesting that they strictly regulate stomatal conductance in response to increases in atmospheric vapor pressure deficit (VPD), argued to be an increasingly important constraint on ecosystem function in the future as global temperatures rise (Novick et al., 2016; Sulman et al., 2016). Other studies argue that anisohydric strategies may be preferred in tropical systems with little risk of water stress (Kumagai and Porporato, 2012) and that Trees − including tropical species − exhibit a range of isohydric to anisohydric hydraulic behaviors (Klein, 2014). Eddy covariance measurements of water and energy flux can help us understand these dynamics at the ecosystem scale. Evapotranspiration from tropical forests is well-known to be energy limited on average (Mallick et al., 2016; Williams et al., 2012), but moisture limitation exists during drought (Gatti et al., 2014). It is also important to understand how seasonal patterns of light and water availability interact with canopy hydraulic behavior to impact water and heat flux from tropical forests (Huete et al., 2006; Morton et al., 2014; Saleska et al., 2016, 2007). Vertical transport via the buoyancy flux − dominated by *H* − is a limiting factor in tropical cloud formation and precipitation (Badiya Roy and Avissar, 2002) and its accurate determination is critical for understanding such processes, which differ among wet and dry seasons. On average, the seasonal patterns of *H* and *LE* tend to be more muted in tropical forests than other global ecosystems, but important differences in energy flux partitioning emerge across the dry and wet seasons at specific sites (da Rocha et al., 2009, 2004; Fuentes et al., 2016; Mallick et al., 2016), which are changing due to shifts in the intertropical convergence zone (Sultan and Janicot, 2000; Voigt et al., 2014; Zeng et al., 2008). Combined, these studies make it clear that improving our understanding of tropical forests in the Earth system requires accurate diurnal and seasonal estimates of *H* and *LE*.

Here, we investigate eddy covariance observations from a tropical rainforest in the central Brazilian Amazon using averaging period and transfer entropy (information flow) analyses to gain insight into the causes of *E* for the purpose of better-understanding diurnal and seasonal patterns of *H* and *LE*. Following studies on mesoscale dynamics, we hypothesize that increasing the eddy covariance averaging period likewise be will be associated with increased values of measured *H*. We further hypothesize that information flow from *H* to *E* will increase during states when mesoscale processes are stronger (e.g. during midday during the dry season), and that this process network signature will help us infer the causes of *E*. We first describe the measurements and techniques used to study the hypotheses and discuss how findings impact our understanding of diurnal and seasonal patterns of *H* and *LE*.

2. Materials and methods

2.1. Site description

Measurements for the energy balance averaging analysis were made as part of the GoAmazon Boundary Layer Experiment, hereafter the "GoAmazon" suite of sensors described in Fuentes et al. (2016), which is part of the US Department of Energy funded Observations and Modeling of the Green Ocean Amazon (GoAmazon 2014/5, Martin et al., 2016). Observations come from the BR-Ma2 tower (also called the K34 tower at ZF2 and designated as T0k during GoAmazon 2014/5) (Araújo et al., 2002; Jardine et al., 2015; Kruijt et al., 2004; Malhi et al., 2002, 1998; Tóta et al., 2012) located in the Cuieiras Biological Reserve at 2.60191°S, 60.2093°W approximately 60 km NNW from Manaus, Brazil and managed by the Brazilian National Institute for Amazon Research (INPA). The tower itself is 50 m tall and located in primary tropical rainforest with characteristic canopy heights on the order of 30–40 m and leaf area index values estimated to be between 5.7 $m^2\ m^{-2}$ and 7.3 $m^2\ m^{-2}$ (McWilliams et al., 1993; Marques Filho et al., 2005; Tóta et al., 2012). The tallest trees near the tower reach 35 m, which we take to be the effective canopy height (*h*). Topography surrounding the tower is characterized by a sequence of plateaus and valleys, with approximate height differences of 50 m across a spatial domain of tens of kilometers.

2.2. Measurements

Turbulent flux quantities necessary for the calculation of *H* and *LE* were measured using a sonic anemometer (model CSAT-3, Campbell Scientific Inc., Logan, UT, USA) for the three wind components (*u*, *v*, *w*) and an open path infra-red gas analyzer (model LI-7500A, Licor,

Lincoln, NE, USA) for water vapor concentrations mounted 48 m (z) above ground ($z\,h^{-1} = 1.37$). The sonic anemometer was facing east, which is consistent with the mean wind direction at the site. Data were saved at 20 Hz on dataloggers (model CR3000, Campbell Scientific). R_n was measured using upward and downward facing pyranometers (model CM21, Kipp & Zonen, Delft, The Netherlands) mounted at 44.6 m for shortwave radiative components as well as upward and downward facing pyrgeometers (model CG3, Kipp & Zonen) mounted at 39 m above ground. Soil heat fluxes were measured using heat flux plates (model HFP01, Hukseflux Thermal Sensors, Delft, The Netherlands). Observed ground heat fluxes (G) were small (about 5 W m^{-2}) compared to the other flux components and their measurement errors (Fuentes et al., 2016). As G was small and there were substantial gaps in data acquisition, G is not included in the calculation of the energy balance for the averaging length analysis. Turbulent flux data used for the averaging period analysis were collected between 04 April 2014 and 16 January 2015. However, due to a lightning strike, the LI-7500A gas analyzer was not operational between 27 May 2014 and 10 October 2014; these periods are excluded from the present analysis of E.

Fluxes were calculated using EddyPro (Licor). Processing involved double coordinate rotation and linear detrending. The moisture correction on the eddy covariance fluxes to compensate for density fluctuations was applied (Webb et al., 1980). Fluxes were quality controlled (Mauder and Foken, 2004) assigning quality flags from 0 to 2, from best to worst data quality. Fluxes with a quality flag of 2 were excluded from subsequent analyses. Flux calculations were performed for averaging periods of 30, 60, 120, and 240 min to investigate the impact of averaging length and thus inclusion of larger scale eddies on flux closure. The analysis focuses on daytime periods, defined here to be 0800-1800 local time. Because of the missing data periods, our analysis of the seasonal variability in information flows from H and LE uses observations from site BR-Ma2 from the FLUXNET LaThuille dataset for which standardized gapfilling methods for H and LE have been applied (Papale et al., 2006). The BR-Ma2 dataset spans from 1999 to 2006. We restrict this analysis to days in which more than half of observations are measured rather than gapfilled.

H and LE are used in combination with the water vapor mixing ratio (q, obtained from the relative humidity in the FLUXNET dataset and ambient pressure measurements at BR-Ma2) and the potential temperature (θ) to estimate the buoyancy flux (HB) according to Stull (1988):

$$HB = \frac{\overline{w'\theta_v'}}{\rho c_p}, \tag{1}$$

$$\overline{w'\theta_v'} \approx \theta[0.61\overline{w'q'}] + \overline{w'\theta'}[1 + 0.61q], \tag{2}$$

with $[\theta_v = \theta(1 + 0.61q)]$ as the virtual potential temperature, the kinematic moisture flux $[\overline{w'q'} = LE/(\rho\lambda)]$, and the kinematic heat flux $[\overline{w'\theta'} = H/(\rho c_p)]$, where ρ is the air density, λ is the latent heat of evaporation for water, and cp is the heat capacity of dry air at constant pressure.

2.3. The energy balance

The energy balance equation, which yields the energy balance residual E, is defined as the difference between R_n and the components of the surface fluxes:

$$E = R_n - H - LE - G, \tag{3}$$

Note that E contains unmeasured metabolic terms as well as heat storage terms (Haverd et al., 2007), as well as any differences between real *versus* measured radiative and turbulent flux terms.

2.4. Using an information flow dynamical process network to diagnose energy balance closure

The FLUXNET BR-Ma2 dataset was divided into sixteen time periods

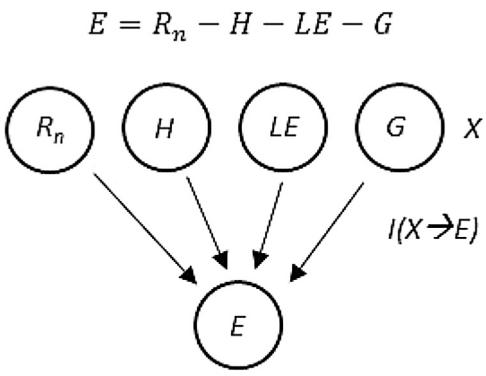

Fig. 1. Schematic illustrating information flow $I(X \rightarrow E)$ from the individual components of the energy balance (R_n, H, LE, G) to the energy balance residual (E).

representing sixteen different "eco-climate states" (Ruddell et al., 2015). Each state is characterized by a potentially unique pattern of turbulent and mesoscale processes, and has a unique process network describing the contribution of each energy balance component (Equation (3)) to the residual error described by E (Fig. 1). We define here the nodes of the process network as the terms in the energy balance equation. We assign the directional weighting of links in the process network as the dynamical mutual information between each pair of terms (or nodes). A stronger link means that more of the energy balance residual is attributable to the energy balance term that is originating the information content. The end result is an Information Flow Dynamical Process Network (IDPN, Ruddell et al., 2015) for this energy conservation equation, and the resulting capability to observe how the energy balance processes affect the energy balance residual.

Mutual information (I) is the simplest and most robust metric for this application (Weijs, 2011), because it quantifies how much information about the energy balance residual term is provided by each term in the observed energy balance. If there were never an energy balance residual (i.e. $E = 0$ W m^{-2}) and the measured energy balance was closed, the dynamical mutual information is zero. More generally, if the energy balance residual takes a steady state (including a steady 0 W m^{-2} value), then the dynamical Shannon entropy (S) and the resulting mutual information is zero by definition (Kang et al., 2017). But, if the residual takes an average value of zero with nonzero variance, there *will* be dynamical mutual information between the residual term and any term that co-varies with the residual and provides Bayesian probabilistic predictability.

This last instance is the most interesting for this study because it most nearly approximates the normal situation for a flux tower, or almost any sensor system. Most measurements systems, including the eddy covariance system, are designed to be accurate with zero average residual error at an acceptable resolution in space and time, but while tolerating finer-resolution (or higher frequency) random and systematic errors that cancel out in the coarse averages. In this case, a good method to infer the source of residual error is the examination of the information content of fine-resolution processes and the closure (or lack thereof) of information content provided by fine-resolution processes. We do this by examining thirty-minute information content in a system where average E approaches zero (within five percent) at timescales of several hours. This method will identify as information flows the sources of error that are attributable to "fast" dynamical and/or random processes that operate at timescales finer than the observations, but will not identify sources of error that are attributable to "slow" processes that operate at timescales slower than observations, or sources of error that are steady-state (non-dynamic) at the timescales in question (Kang et al., 2017). If all sources of the energy balance residual error are perfectly identified and attributed as information flows at the chosen timescale and resolution using the chosen methods, then the information closure $C = 1$; if the sources of error are attributable as informa-

tion flows to unobserved processes or timescales, $C \neq 1$. A more detailed discussion of information closure is provided in Appendix A.

The dynamical mutual information I between variable X and Y is $I_{a,\Delta,\tau,\Delta s}$ and is more generally expressed specific to a system state a, a minimum resolution Δ_X or Δ_Y, a process time lag τ, and a time scale Δs, given a dataset time resolution Δt. Here, we use the distribution-normalized mutual information that falls between zero and one, with eleven equal width bins that are defined against the global range of variation within the dataset, zero time lag ($\tau = 0$), a time scale of 30 min ($s = 30$ min), and use no anomalies or other pre-filtering techniques on the time series data, per the dynamical information flow techniques defined by Ruddell and Kumar (2009a), Kang et al. (2017), and Sturtevant et al. (2016). This binning scheme yields a minimum resolution of dynamics defined by the bin widths (in units of W m^{-2}) of 129.6 for E, 103 for R_n, 101.3 for LE, 72.2 for H, and 3.2 for G; this bin width is adequate to capture the major dynamics of the energy balance terms and is a good balance between precision and data requirements to calculate S (Kang et al., 2017). The number of data used for each calculation ranges from 269 to 825 observations, which is enough for qualitatively robust estimation of I (Paninski, 2003; Ruddell and Kumar, 2009a). A time lag of zero and time scale equal to the time resolution of the data are the best default choices for this analysis because we know by definition that the energy balance terms and processes are summative at this lag and time scale.

The sixteen system states (Ruddell et al., 2015) are combinations of four times of day and four seasons of the year. Four two-hour windows (local time) were chosen that comprise the core of the sunlit daytime hours in a tropical forest: 0800–1000 (morning), 1000–1200 (late morning), 1200–1400 (early afternoon), and 1400–1600 (afternoon). Four seasonal periods traverse the seasonal precipitation regimes and the resulting shifts in dryness and Bowen ratios: Wet season (Wet), dry season (Dry), and transitions from Wet to Dry and Dry to Wet. We choose these sixteen states to study different information flow signatures that may correspond to different turbulent and mesoscale energy transport processes affecting the energy balance residual, and focus on Wet and Dry seasons to best understand seasonal contrasts.

3. Results

3.1. Seasonal patterns in energy partitioning

To understand how insights from averaging period and information flow analyses impact our understanding of the seasonality of measured surface-atmosphere exchange, we must characterize observed fluxes. The annual behavior of R_n has two distinct maxima (Fig. 2). The first occurs around mid-January (DOY = 19), while the second one occurs near the end of August (DOY = 237) during the dry season, which typically lasts from July to September, but shows considerable inter-annual variability (Hodnett et al., 1995). H and LE show contrasting behavior during both periods with (relatively) high R_n. H and LE increase in response to R_n more in the dry season than the wet season (Fig. 2). Day-to-day variability in LE can reach 3 MJ m^{-2} d^{-1} and is much larger than for H, which is typically smaller than 1 MJ m^{-2} d^{-1}. While both H and LE follow the seasonal pattern in R_n, periods of low R_n are often followed by rapid increases in LE. In consequence, there is considerable day-to-day variation in β (Fig. 3), which tends to range from 0.2 to 0.4. H reacts more strongly than LE to the annual pattern of R_n as β gradually increases from 0.25 in April to 0.4 at the end of September, and increases more strongly as a function of R_n, especially during the dry season (Fig. 4). During the transition towards the wet season in October, β declines again towards 0.25.

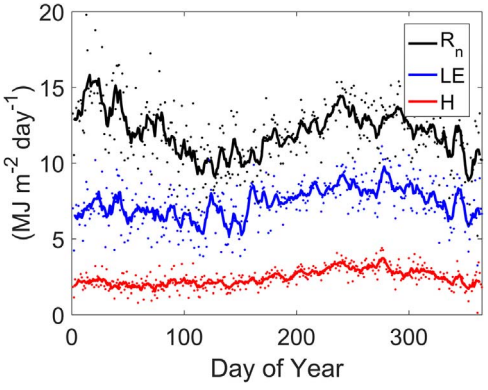

Fig. 2. Seasonal patterns of net radiation (R_n), latent heat (LE), and sensible (H) heat fluxes at the BR-Ma2 study ecosystem in the central Amazon calculated using the LaThuille FLUXNET dataset (1999–2006). Thick lines are the result of a seven-day moving filter.

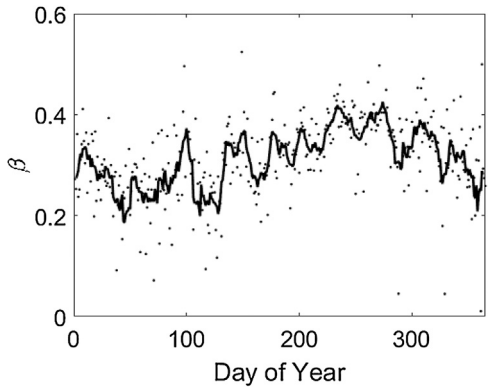

Fig. 3. Seasonal patterns of Bowen-ratio ($\beta = H/LE$) at the BR-Ma2 study ecosystem in the central Amazon calculated using the LaThuille FLUXNET dataset (1999–2006). The thick line is the result of a seven-day moving filter.

Even though E is inversely related to R_n (Fig. 5), variation of R_n itself explains only a small portion of the variance of E. As R_n in tropical environments is mostly governed by cloud cover rather than seasonal differences in insolation, we divided the data into dry and wet season fluxes (Fig. 6). During the dry season, the diurnal maximum R_n is approximately 100 W m^{-2} greater than during the wet season. As a consequence, both H and LE are greater as well. The absolute magnitude of E between seasons is similar, so that wet season E is comparable in magnitude to H. E is large during the morning hours and then declines together with H during the afternoon for the wet season, while dry season E plateaus in the late afternoon.

3.2. Averaging period analysis

Following the methodology outlined in Malhi et al. (2002), diurnal

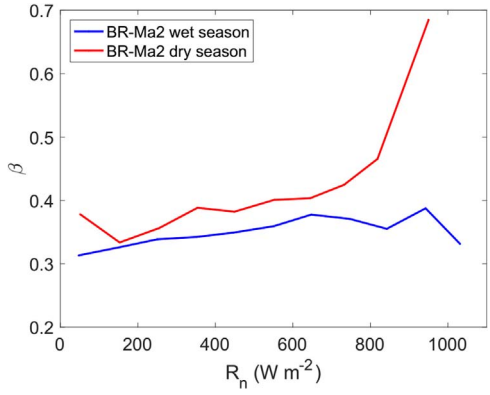

Fig. 4. Seasonal patterns of the response of the Bowen ratio (β) − the sensible heat flux divided by the latent heat flux − to net radiation (R_n) at the BR-Ma2 study ecosystem in the central Amazon across the wet and dry seasons calculated using the LaThuille FLUXNET dataset (1999–2006).

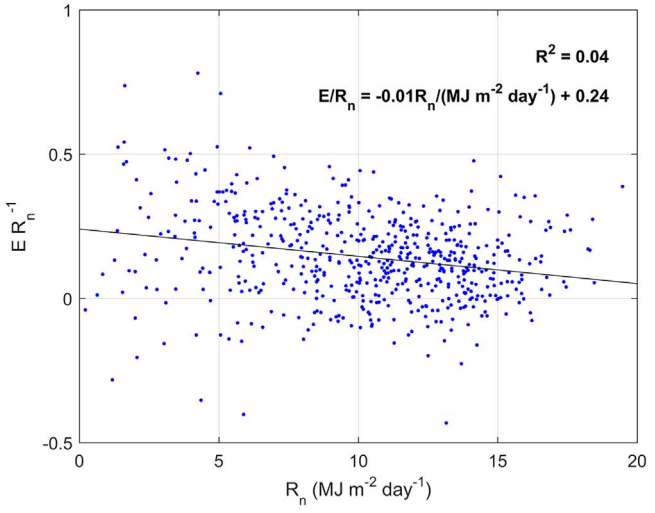

Fig. 5. Daily integrated energy balance residual (E), normalized by daily integrated net radiation (R_n) at the Br-Ma2 tropical forest as function of R_n calculated using the LaThuille FLUXNET dataset (1999–2006) The black line idicates a linear best fit to the data.

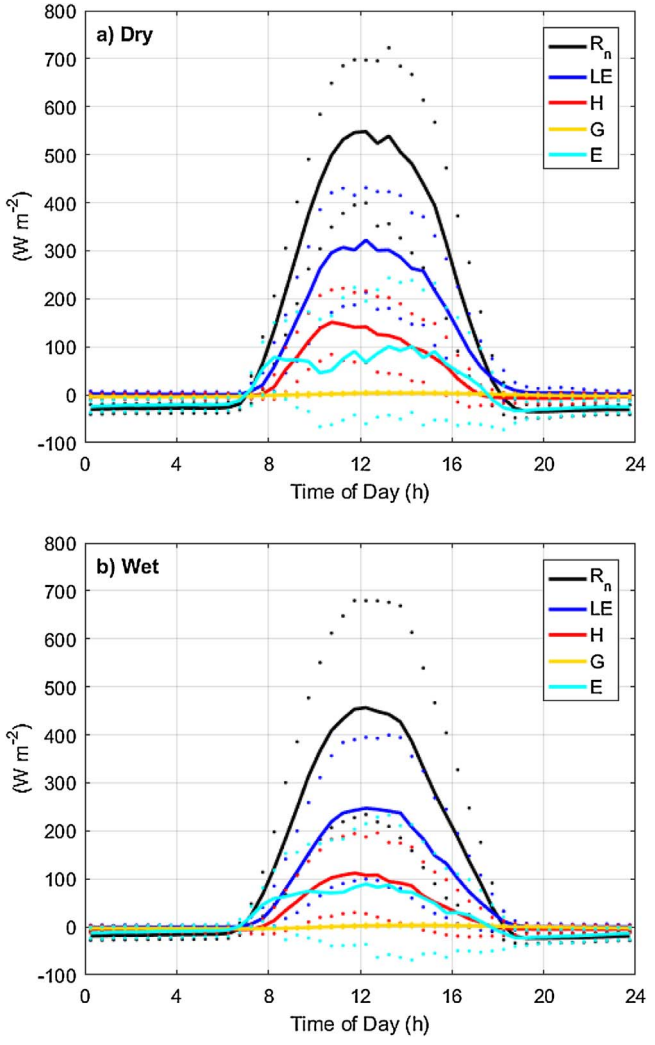

Fig. 6. Terms of the energy balance equation for 30-min averaging lengths as defined in the text for dry (a) and wet (b) season (defined in text) for the FLUXNET Br-Ma2 dataset calculated using the LaThuille FLUXNET dataset (1999–2006). The dots indicate the standard deviation of fluxes.

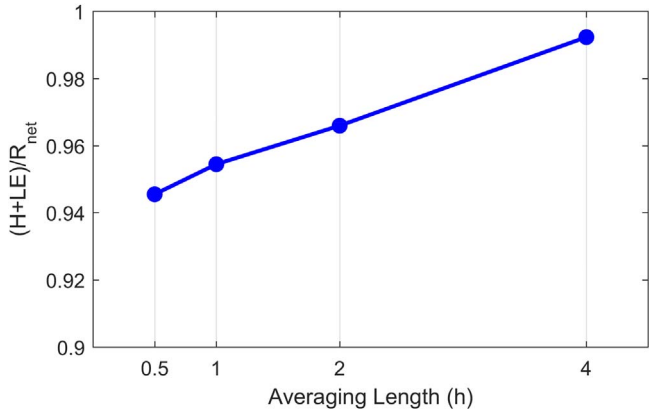

Fig. 7. Diurnal energy balance closure at a tropical rainforest in the central Amazon at BR-Ma2 during 2014 using increasing averaging lengths following Malhi et al. (2002).

integrals of *H* and *LE* were compared to the integrated R_n. Such processing on the diurnal scale minimizes storage changes of heat as a source of uncertainty (Leuning et al., 2012), but limits the analyis to days without gaps in flux measurements. Overall, increasing the averaging length from 0.5 to 4 h leads to almost complete closure of the energy balance. Diurnal eddy covariance energy balance closure was 94.6% for the conventional 0.5 h averaging period and 99.2% with the 4 h averaging period (Fig. 7). Note that this analysis was performed without application of any quality control to the calculated fluxes, as increasing averaging lengths will lead to a violation of the stationarity criterion for the eddy covariance method.

Subsequent analysis of quality controlled daytime fluxes shows increasing instantaneous energy balance closures in the afternoon (1400–1600 and 1600–1800, i.e. decreasing *E*) for increasing the averaging lengths from 0.5 to 2 h (Fig. 8). A further increase from 2 to 4 h had little effect on the overall energy balance closure, and no such effect was found for the morning hours. This increase in energy balance closure is associated with increasing β, indicating a rising share of *H* to the overall turbulent flux. Values of β observed during the 2014 wet season were generally lower than 0.5 and thus smaller than β observed by Malhi et al. (2002) in the range of 0.5–1.1.

Additional analysis reveals contrasting behavior between *H* and *LE* during morning and afternoon hours (Fig. 9). *H* increased by 30% from 103 W m^{-2} (0.5 h averaging time) to 131 W m^{-2} (4 h averaging time) during the morning (0800-1200), while the corresponding *LE* decreased by a lesser amount (333–312 W m^{-2}) upon an increase in averaging time. The change in *H* arose largely from the 0800-1000 period, when it increased upon the two hour averaging time. In the afternoon (1200–1600), changes in turbulent fluxes as a function of eddy covariance averaging period were less pronounced for *H* (76–69 W m^{-2}) and negligable for *LE* (355–357 W m^{-2}), and appear only after increasing the averaging period length from 2 to 4 h.

3.3. Information flows to the energy balance residual

3.3.1. Dry season

The information flow analysis during the dry season (Fig. 10) reveals that R_n and *LE* have the highest information flow to *E*: $I(R_n \rightarrow E)$ and $I(LE \rightarrow E)$. At 0800, $I(R_n \rightarrow E)$ is the dominant term of information flow and then declines over the course of the day explaining between 10 and 15% of the residual error's Shannon Entropy *S(E)*. $I(LE \rightarrow E)$, which explains between 7% and 15% of *S(E)*, increases approximately by a factor of 2 from 0800 to 1000 and then decreases in the afternoon, while $I(H \rightarrow E)$ exhibits a peak at 7% of *S(E)* in the afternoon. The information flow from the ground heat flux, $I(G \rightarrow E)$, has the smallest information flows (typically below 5%), reflecting the relatively small magnitude of the ground heat flux and also this flux's relatively small rate of change at 30 min timescales. The total informa-

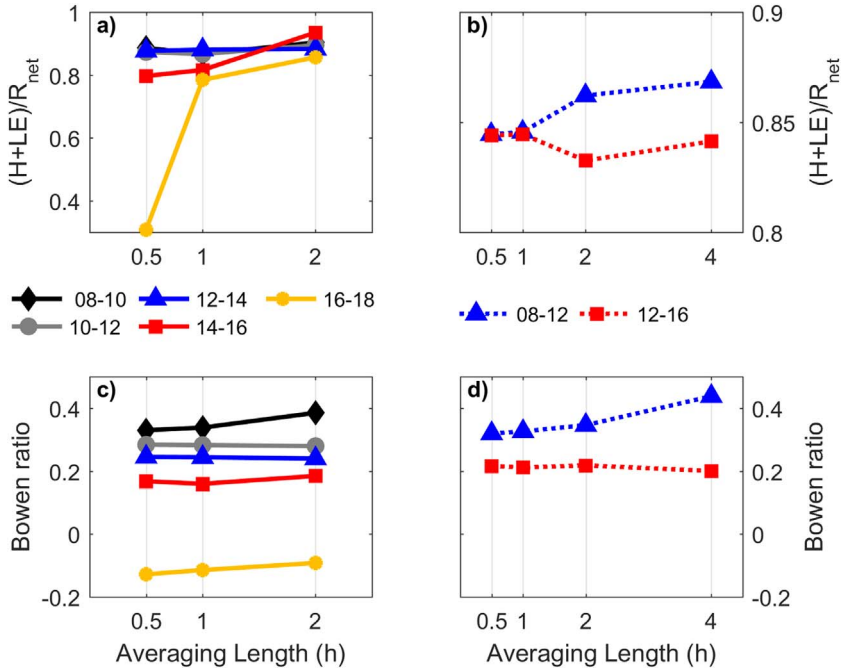

Fig. 8. Energy balance closure ratio defined here as the sum of sensible (*H*) and latent heat flux (*LE*) divided by the net radiation (R_n) at the BR-Ma2 eddy covariance flux tower in the central Amazon during 2014 using increasing averaging lengths from 0.5 to 4 h and for different times of day for (a) for averaging lengths up to 2 h and (b) for averaging lengths up to 4 h during morning (0800 until 1200, local time) and afternoon (1200–1600) periods. Subplots (c) and (d) are the same as (a) and (b) but for the Bowen ratio.

tion flow from R_n, *LE*, *H*, and *G* to *E* is expressed as the Information Closure *C* [$C = \Sigma_X$ I(X → E)/S(E)]. *C* is largest in the intervals before and after noon, around 40% at 1000. *C* is approximately 35% at 1400, while *C*-values during 0800 and 1400 are approximately 10% smaller. During the dry season the information flow from *HB* to *E* is 30–50% larger than *I(H → E)*, despite the fact that the *HB* flux exceeds *H* by only 10–16%. The minimum in *C* during the late afternoon coincides with the diurnal precipitation maximum and the highest β (Fuentes et al., 2016). At the same time, vapor pressure deficits, which can exert control on evapotranspiration, during the afternoon are also largest, highlighting the discrete nature of precipitation events and the diurnal drying of the ABL due to mixed-layer growth and entrainment of dry air from the free-troposphere. Afternoon rainfall events threrefore reduce information closure in the afternoon during the dry season by introducing energy flux processes that are not observed by the eddy-covariance measurement system.

3.3.2. Wet season

While the general behavior of the information flow during the wet season is similar to the dry season, there are notable differences (Fig. 11). Due to increased cloud cover, R_n is decreased, which leads to smaller *LE*, *H*, and *E*, while β decreases by approximately 0.05

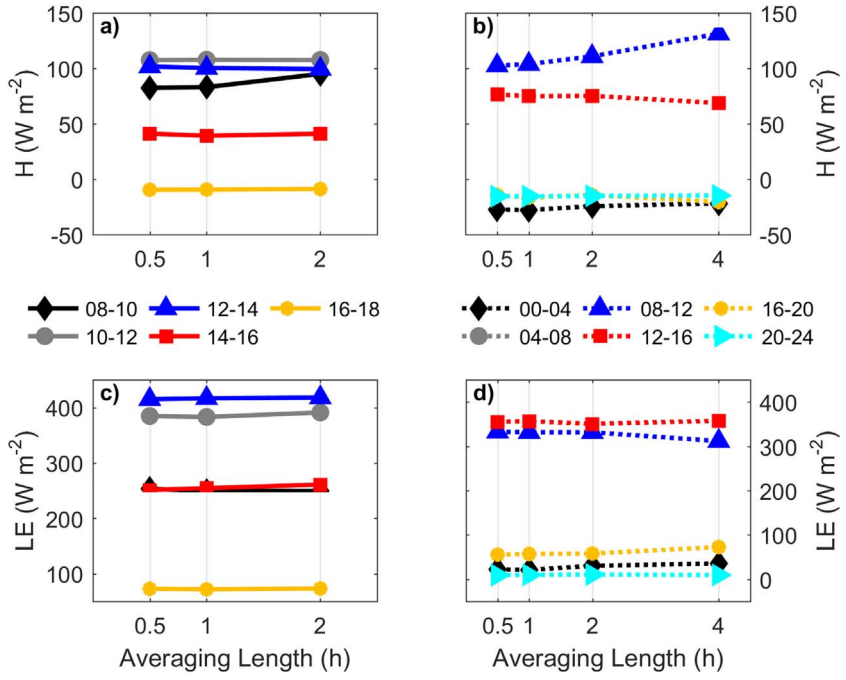

Fig. 9. As Fig. 8, but displaying sensible (a & b) and latent heat (c & d) fluxes for averaging times from 0.5 to 4 h.

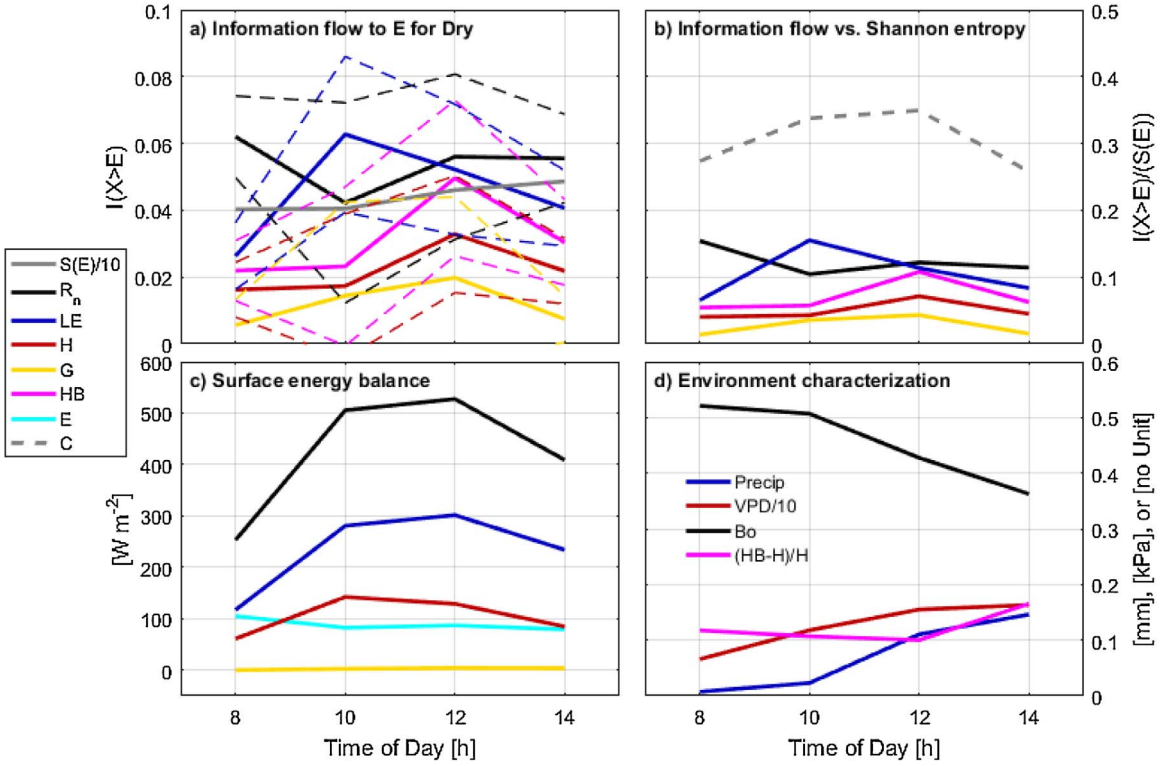

Fig. 10. Information flow analysis for the dry season (defined in text): (a) Information flow to the energy balance residual $I(X \rightarrow E)$ from individual components of the energy-balance (R_n, H, LE, G), estimated buoyancy flux (HB) [W m^{-2}] and Shannon entropy ($S(E)$) during the dry season (defined in text); (b) Information flow compared to Shannon entropy, with C as the closure ratio between the total information flow from R_n, H, LE and G to Shannon entropy; (c) terms of the surface energy balance including observed residual (EBR); and (d) characterization of the environmental conditions such as precipitation (Precip), vapor pressure deficit (VPD), Bowen ratio and relative difference of buoyancy flux to sensible heat flux ($(HB\text{-}H)/H$). Dashed lines indicate 95% confidence intervals.

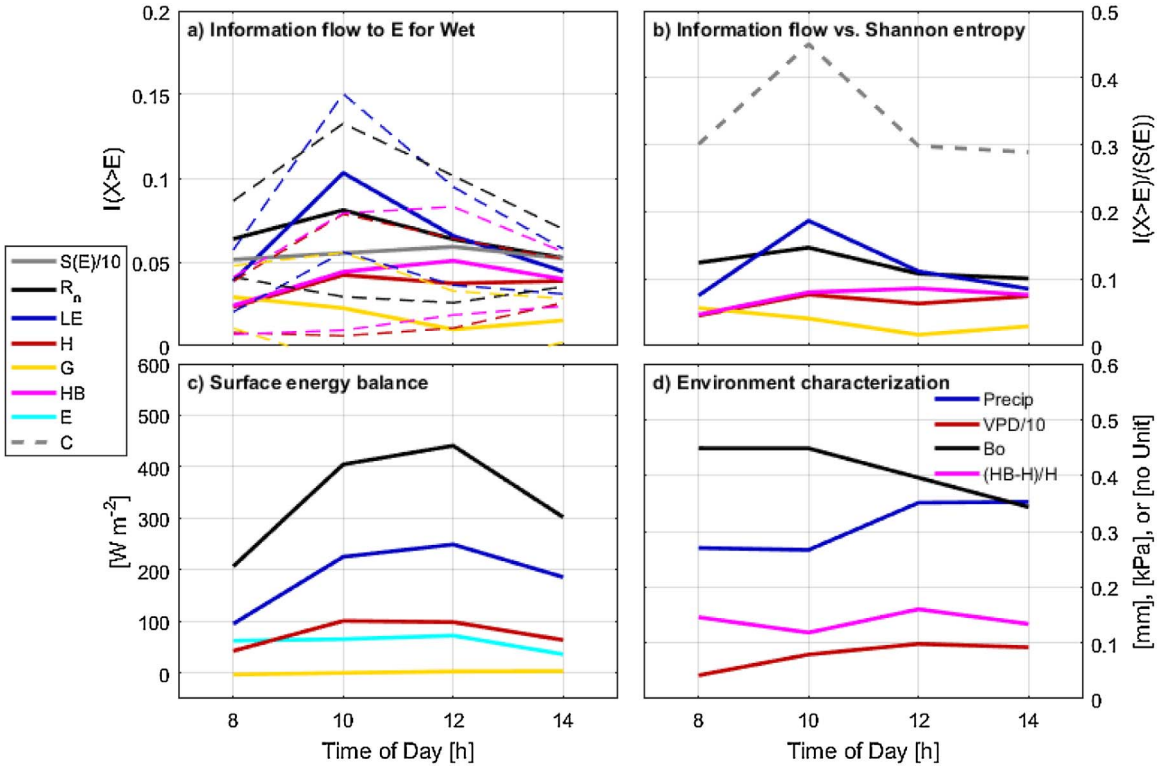

Fig. 11. Information flow analysis for the wet season (defined in text): (a) Information flow to the energy balance residual $I(X \rightarrow E)$ from individual components of the energy-balance (R_n, H, LE, G), estimated buoyancy flux (HB) [W m^{-2}] and Shannon entropy ($S(E)$) during the wet season (defined in text); (b) Information flow compared to Shannon entropy, with C as the closure ratio between the total information flow from R_n, H, LE and G to Shannon entropy; (c) terms of the surface energy balance including observed residual (E); and (d) characterization of the environmental conditions such as precipitation (Precip), vapor pressure deficit (VPD), Bowen ratio and relative difference of buoyancy flux to sensible heat flux ($(HB\text{-}H)/H$). Dashed lines indicate 95% confidence intervals.

compared to the dry season throughout the day. The Shannon entropy of the energy balance residual *S(E)* during the wet season is higher than during the dry season (0.5-0.6 in wet vs 0.4-0.5 in dry). *C*, which is dominated by information flows from *LE*, reaches its peak of 45% at 1000. In contrast to the dry season, there is almost no difference between $I(HB \rightarrow E)$ and $I(H \rightarrow E)$ during the wet season, despite the fact that the estimated difference between the *HB* and *H* fluxes is larger during the wet season than the dry season. Precipitation is significantly higher in the wet season compared to the dry season, which is associated with a drop in the Shannon entropy of the energy balance residual *S(E)* at 1400 during the wet season. Rainfall appears to cause a greater disruptions to energy balance observations during the wet season's afternoons than during the dry season's afternoons, probably because of the higher rainfall totals.

4. Discussion

4.1. Seasonal patterns in energy partitioning

Due to its location near the Equator, the highest potential solar irradiance at the BR-Ma2 site occurs close to the equinoxes in March and September (Malhi et al., 2002). While R_n displays a maximum in September, March coincides with its annual minimum, highlighting the importance of cloud cover for the dynamics of R_n. Evapotranspiration in tropical forests is generally assumed to be limited by the available energy (Mallick et al., 2016; Williams et al., 2012) and a close relationship between R_n and *LE* is thus expected. Such a relationship is clearly detectable on the seasonal scale (Fig. 2). At the same time, the large sub-seasonal variability in *LE* and the associated fluctuations in β (Fig. 3), indicates the importance of additional processes. On several occasions (e.g. DOY 118 or 271), local minima in R_n, likely associated with cloud cover and precipitation are directly followed by sharp increases in *LE*, highlighting the importance of moisture availability for flux partitioning even for a tropical forest. The range of Bowen ratios reported in this work is considerably lower than the previously reported range of 0.5-1.1 (Malhi et al., 2002). A potential explanation for this discrepancy may be attenuation of water vapor fluctuations caused by the closed path setup by Malhi et al. (2002) and the longer extent of the LaThuille dataset for BR-Ma2 used to describe seasonality of turbulent fluxes here, which reduces the impact of inter-annual variability in environmental conditions.

From this standpoint it is critical to acknowledge the important role of instrumentation for the energy balance closure; data from the LaThuille dataset explored by Stoy et al. (2013) from BR-Ma2 had an energy balance closure of 85% (see also Fig. 5) and energy balance closure from the present study (using the GoAmazon suite of sensors) is in excess of 94% depending on averaging period length. If *H* is in fact primarily responsible for lack of energy balance closure during daytime convective conditions, we would expect β to increase from the averaging period analysis. This is indeed apparent during periods of high *H* and R_n (Figs. 2 and 4). The weak dependency of *E* on R_n, highlights the importance of additional environmental processes on *E* that we explore here. Combining Figs. 5 and 6, shows that the seasonality of fluxes and thus also of *E* is in large part driven by R_n, which is closely associated with cloud cover rather than traditional climatological seasons. Nevertheless, there is large day-to-day variability, which causes large deviations from the mean states. The strong and persistant early morning increase of *E* (Fig. 6) is likely caused by energy flow into canopy storage. The diurnal behavior of *E* for the wet and dry season diverges most during the afternoon hours, which is further explored in section 4.3.

4.2. Averaging period analysis

E continues to present a problem for accurately estimating the Earth's surface energy balance and thereby the magnitude of *H* and *LE* that affect Earth system processes. Non-orthogonal sonic anemometer design (Frank et al., 2013; Kochendorfer et al., 2012) and low frequency contributions to *H* and *LE*, such as mesoscale circulations (Foken, 2008; Foken et al., 2011) are widely assumed to be the main causes of an underestimate of turbulent flux terms and thereby *E*. With respect to the latter mechanism, as mesoscale motions occur on frequencies that cannot be captured in short averaging periods, extending the integration time from 30 min to several hours has been proposed as a potential solution. Our findings show that extension of the energy balance from 30 min to 4 h (and as a consequence disregarding the stationarity assumption of the eddy covariance method) closes the energy balance at a tropical forest research site and that an increase in *H* with longer averaging periods is largely responsible for reducing *E*. These findings suggest that energy balance closure at BR-Ma2 is impacted by exchange processes such as very large eddies and mesoscale motions with timescales larger than 30 min, which are found to disproportionally affect *H*. Findings are in agreement with Malhi et al. (2002), who also reached closure after 4 h using independent measurements at the same site. However, other studies (e.g. Foken et al., 2006) did not find decreases in *E* for such averaging times, highlighting the importance of site specific conditions and processes on energy-balance closure. The increased closure for longer averaging length indicates that sonic anemometer errors, which should not be affected by averaging length, do not seem to significantly influence results at the study site. The obvious drawback of extended flux integration times is the requirement of stationary conditions for the eddy covariance method, which is typically invalid for averaging times exceeding 60 min.

For long-term applications and comparison to surface-vegetation-atmosphere transfer (SVAT) models, which enforce energy balance closure (Kracher et al., 2009), *E* is often addressed by distributing the energy-balance residual to sensible and latent heat fluxes according to β (Twine et al., 2000). However, such correction techniques do not address the underlying mechanisms of *E* and simply assume that unmeasured fluxes behave like measured fluxes, which is a reasonable assumption in the absence of other information. The increasing β associated with the increase in flux closure are supported by the findings of Charuchittipan et al. (2014), who concluded that scalar similarity between *H* and *LE* does not hold for mesoscale circulations, which contributed significantly to overall energy transport. It was also found that such circulations transported more *H* than *LE* near the surface. Tóta et al. (2012) reported persistent buoyancy driven flows above and below the canopy in the vicinity of BR-Ma2. During the daytime, buoyancy driven flows above the canopy were upslope, indicating flux convergence at the K34 tower, located on a plateau. It is likely that the proportionally largest increase in energy balance closure, observed in the late afternoon before sunset, is the result of decreasing turbulent fluxes, while the buoyancy driven circulation responds more slowly to decreasing solar radiation.

The observed changes in β are most pronounced in the morning (0800-1000) and the two hours preceding sunset. In both cases, *H* increases at a higher proportion than *LE*, which changes little. Kruijt et al. (2000) documented that nighttime temperatures inside the BR-Ma2 canopy exceed above canopy temperatures, and that heat exchange between the canopy and the atmospheric surface-layer is limited by an inversion layer (Santos et al., 2016). In the absence of sufficiently strong turbulence during the early morning hour this inversion persists. Freire et al. (2017) have shown a strong increase in turbulent scalar transport after sunrise for the upper canopy, while lower portions of the canopy remain in a partially mixed regime. Future studies should investigate the possibility of upslope mesoscale circulations in the morning that may contribute to an increase in heat exchange between the warmer within-canopy air and the surface-layer and thus increase *H*.

The mechanism for the decrease in *LE* for the 0800-1200 period, however, is unclear. As the canopy presents the major source of

moisture and thus latent energy, enhanced vertical exchange would likely result in an increase of the flux. At the same time, mesoscale circulations can also be associated with the advection of drier air that is unmeasured by an eddy covariance system at a single point. There is substantial spatial heterogeneity in vegetation structure and composition between valleys and plateaus, which may be associated with different evapotranspiration responses.

4.3. Information flow

4.3.1. BR-Ma2

The diurnal evolution of information flow to E shows a consistent behavior between the dry and the wet season (Figs. 10 and 11). In the morning, R_n is the dominant information source to E. One potential explanation for this is the fact that storage changes of energy are not accounted for in the FLUXNET dataset or the GoAmazon suite of sensors (e.g. canopy and air space energy storage is excluded), so that the initial flow of energy into canopy storage appears as contribution to the energy-balance residual. The information flow from LE peaks before noon and then declines in the afternoon so that R_n again dominates information flow to E, while the information flow from H shows no clear trend throughout the day. When comparing wet to dry season, two main differences in the diurnal dynamics can be detected.

First, the Shannon entropy of the energy balance residual $S(E)$ is considerable during the dry season and increases during the day. In contrast, during the wet season, the peak of $S(E)$ occurs for the 1200–1400 interval and then decreases in the late afternoon. The timing of maximum $S(E)$ is consistent with the diurnal precipitation and R_n maxima (Fuentes et al., 2016) and may also be associated with the generally higher afternoon cloud cover during the wet season. During the dry season, convective precipitation at the site exhibits a clear diurnal maximum between 1400 and 1600 (Fuentes et al., 2016). A similar rainfall maximum during the wet season is much less apparent and occurs earlier in the day. The 1000 interval during the wet season is characterized by a simultaneous maximum in $I(LE \rightarrow E)$ and $I(R_n \rightarrow E)$. A small peak is also seen for $I(H \rightarrow E)$. It can be hypothesized that in the tropics, where seasonality is less pronounced than non-tropical ecosystems both R_n and thus turbulent fluxes are primarily regulated by cloud cover. Hence the maximum in information flow at 1000 may reflect the system's radiative response to changes in cloud cover. Higher dry season S means that fast-timescale dynamic and random energy balance error processes are more prevalent during the dry season, especially in the afternoon. During the wet season, the energy balance residual may be relatively more attributable to slow-timescale and unobserved processes than to random errors, as compared with the dry season.

The second seasonal difference is found in the behavior of the information flow related to HB and H. During the dry season, $I(HB \rightarrow E)$ is significantly larger than $I(H \rightarrow E)$, while no such difference exists for the wet season. The difference between $I(HB \rightarrow E)$ and $I(H \rightarrow E)$, which reaches its peak between 1200 and 1400, is larger than the difference between HB and H itself, indicating an elevated importance of HB compared to H on the information flow to E.

Overall, the closure of the information flow remains below 50% throughout the daytime and seasons, indicating that the analysis does not capture all relevant processes that contribute to E at 30-min timescales. The magnitude of the information flows mostly stacks with the magnitude of the corresponding component of the energy balance, which can be explained by 'random' fine-scale errors, associated with the flux and radiation measurements, contributing to E. In consequence the information flow analysis does not produce conclusive results to elucidate the relative importance of H and LE to the non-closure of the energy balance. Nevertheless, the behavior of energy transfer during the dry season appears to be consistent with the arguments of Charuchittipan et al. (2014) due to the fact that mesoscale flows at the BR-Ma2 site should be more prevalent during the dry season and that there appears to be an over-proportional contribution of HB to E. The processes analyzed in this work only explain between 25% and 45% of the total Shannon entropy. However, complex environmental systems such as the Amazon rainforest, not only have a multitude of environmental factors and rapidly changing environmental conditions that can affect the energy balance residual, but also provide a challenging environment for data collection.

4.3.2. General considerations for information closure

A limitation of the original process network method proposed by Ruddell and Kumar (2009a) is that it is not possible in an open system to be certain that all of the important variables and processes are included in the analysis. In the context of a conservation equation, this limitation is overcome because we are confident by definition that all important variables and processes are included in the conservation equation – albeit not without theoretical and observational uncertainty, or limited precision and resolution (note that technically speaking the energy balance equation used in this work (Eq. (3)) assumes that the impacts of energy storage in vegetation, energy storage due to metabolism, as well as advection are included in E). By applying the discipline of a conservation equation to the selection of variables and processes to include in an IDPN analysis, we gain clarity and precision, and can use this technique to diagnose the exact sources of observational and theoretical uncertainty in a conservation equation. This diagnostic can be extended to the examination of time lag, time scale, and resolution, which re recommend for future analyses of energy balance closure.

It also follows that information is conserved when an IDPN is applied to a conservation equation, and that there is an analogy in this context between the conservation of information and the parallel conservation of mass, energy, momentum, etc. Steady-state conservation systems will have zero dynamical information flow, conserving information. Conservation systems with time dynamics will have information flows between all terms that are non-steady-state (including the residual term) and all information which is created is also consumed on the IDPN (Ruddell and Kumar, 2009b). Of course, the mutual information applied in this paper is only an approximation of the true information flow on the IDPN. The "true" information flow is a conditional mutual information that is free from bias introduced by bin-edge, finite-data, state-edge, and numerous other practical estimation problems, and which also properly separates independent from redundant and synergistic information flows (Goodwell and Kumar, 2015). See Appendix A for further discussion of information closure on a conservation equation.

5. Conclusions

The eddy covariance technique is widely assumed to be the most promising method to obtain long-term ecosystem-atmosphere exchange measurements, which are key for understanding land-atmosphere interactions in a changing climate. Therefore, we must understand E and the and make an explicit attempt to attribute its causes. This work shows that for a tropical rainforest, energy balance closure can be achieved through extension to 4 h averaging length, and that closure is associated with an increase in H as the averaging time is lengthened. At the same time, such an averaging period obscures important aspects of the diurnal cycle that occur at faster time scales. Investigations at this site – and perhaps others – must balance a compromise between energy balance closure and measurements of diurnal flux dynamics. Increasing the integration time of flux calculation leads not only to closure of the energy balance, but also increases the observed daytime β values. These increases occur particularly after sunrise and before sunset and are consistent with the energy transport signature of mesoscale circulations described by Foken et al. (2006) and supports the notion of a flux correction which uses HB following Charuchittipan et al. (2014).

At the same time, process network analysis showed that all

components of the energy balance contribute to E, and that LE and R_n were dominant in the morning, likely due to their role in determining changes in energy storage and cloud cover. During the dry season a more pronounced increase in the information flow of HB compared to H to the E may be associated with heightened convective activity and mesoscale motion, but we cannot exclude contributions from R_n and LE to E. Additionally, the information flow from the energy balance components (R_n, LE, H, G) to E explains less than 50% of the Shannon entropy and the information flows stack similar to the magnitude of the flux components. These results point to additional sources of uncertainty not captured in the flux data and random measurement errors contributing to E. Overall, this work shows that flux analysis and statistical methods can help in better understanding flux dynamics and sources for the E at the site and therefore assist in developing processing methods that can help to improve long term flux datasets and products. Importantly, it demonstrates that a single approach for estimating E may be incomplete, suggesting that multiple techniques for estimating E are required for an integrated understanding of the processes that are responsible for the unclosed surface energy balance.

Acknowledgements

The U.S. Department of Energy supported the field studies as part of the GoAmazon project (grant SC0011075). Fundação de Amparo à Pesquisa do Estado de São Paulo (FAPESP) and Fundação de Amparo à Pesquisa do Estado do Amazonas (FAPEAM) funded the Brazilian component of the field studies. The Large scale Biosphere-Atmosphere Experiment in Amazonia (LBA) provided logistic support and made the flux tower and housing unit available to complete the field studies. PCS acknowledges contributions from the U.S. National Science Foundation [grant numbers 1552976 and 1632810]; JDF acknowledges support from U.S. National Science Foundation (grant 1417914); BLR acknowledges EF-1241960. The opinions are those of the authors, and not necessarily the funding agencies. This work used eddy covariance data acquired and shared by the FLUXNET community, including these networks: AmeriFlux, AfriFlux, AsiaFlux, CarboAfrica, CarboEuropeIP, CarboItaly, CarboMont, ChinaFlux, Fluxnet-Canada, GreenGrass, ICOS, KoFlux, LBA, NECC, OzFlux-TERN, TCOS-Siberia, and USCCC. The FLUXNET eddy covariance data processing and harmonization was carried out by the ICOS Ecosystem Thematic Center, AmeriFlux Management Project and Fluxdata project of FLUXNET, with the support of CDIAC, and the OzFlux, ChinaFlux and AsiaFlux offices.

Appendix A

Begin with a physical conservation Eq. (A.1), describing the conservation of mass, momentum, or in this case energy, expressed explicit for timestep t, such that there is some set of timeseries R_t = {x1, x2, …, xn} of right hand terms that sum to equal the left hand term timeseries L_t at all steps of time. In this paper, $L = +E$, the energy balance residual, and $R = \{+R_n, -H, -LE, -G\}$. Obviously, the terms L and R share identical units; in this paper, the units are [W m^{-2}]. By definition, the terms x in R are physically independent, but they may not be informationally independent.

$$L_t = \sum_{x \in R} x_t \tag{A.1}$$

The analogous information conservation equation gives the Information Closure C (A.2), which is the sum of all information flows $I(X \rightarrow L)$ from right hand terms R to the left hand term L, conditional on any and all independent, redundant, or synergistic information, and specific to a scale and location and resolution and time lag in space and time, etc.

$$C(L) = \sum_{x \in R} I(x \rightarrow L) \tag{A.2}$$

This information flow is most usually a conditional mutual information, and has arbitrary units that correspond to the base of the logarithm used for the calculation of S. Note that a "global" bounding condition across all L, R, and t must be utilized to establish a state-space model (or binning scheme) that treats all information flows equally regardless of the relative magnitude the various x's. C will be zero if L takes a steady state in time (or close enough to steady state, given the finite precision of the binning scheme used for the Dynamical Shannon entropy calculations, see Kang et al., 2017). $I(x \rightarrow L)$ will be zero if either x or L takes a steady state.

C is divided by the Shannon entropy of L, $S(L)$ to yield a dimensionless value C' that is the fraction of $S(L)$ that is explained by the set R (A.3).

$$C'(L) = \frac{C(L)}{S(L)} = \sum_{x \in R} I_R(x \rightarrow L) \tag{A.3}$$

C' is equivalent to summing over all Relative Mutual Information flows I_R from set R to L. For clarity and simplicity, this paper utilizes the dimensionless fractional form of the Information Closure and omits the hash mark. If this $C = 1$, and assuming that (a) our method for calculating I is perfect and that (b) our conservation equation is perfect, then we can say that the information flow from set R fully explains the time-variability of L, and we have a measurement of the relative contribution of each x in R to the variability in L; that is, we can say that "the information is closed".

Information will usually not be closed in a real-world system, and that is why we would use such a formulation: to study the causes of the lack of closure. The Missing Information fraction is M, where $M = 1–C$ (note that this unitless quantity is different from E, defined here to have units of W m^{-2}). $M \neq 0$ for several reasons including, (1) obseration error in the timeseries, (2) improper conditioning in the mutual information such that redundant or syntergystic information confounds the marginal information flows from each x (i.e. x's are informationally non-independent), (3) writing a conservation equation where the terms x are physically non-independent (e.g. in the case where the sensible and latent heat fluxes are physically related through a complementary relationship), (4) using only an insufficient part of the space-time scales or lags that capture the relevant processes, or (5) we are including "disinformation". In this last instance, or for reasons of double-counting of redundant information, we could see $M < 0$. The trick for the use of this method is to design an experiment that allows us to isolate the cause of Missing Information among these many possible causes.

There are several components of this missing information, such that $M = M_e + M_u + M_c + \ldots$, where M_e is the Missing Information due to Estimation Error, M_u is the Missing Information due to uncertainty in the observed or calculated data, M_c is the Missing Information due to conceptual errors in the conservation equation, and "…" is any other source of mising information. We know based on our experience that finite-data and finite-precision limitations generally cause the S to be overestimated, and this often translates in practice into overestimation of the Conditional Mutual Information and $M_e < 0$. Unfortunately, there is no way to constrain M_e in general, except for analytical special cases. Conceptual error will often take the form of lumping together two or more independent processes into a single term, as when the turbulent and buoyancy sensible heat

fluxes are combines. This error may state the information flow from the lumped term as being smaller than the sum of independent information flows from the two terms, so this would result in $M_u > 0$. However, these generalities will not always hold. Developing reliable constraints on *Me, M_u, and M_c*, and versions of these constraints that are explicitly applicable to a specific system state and scale of space and time, is therefore important for the practical application of the information closure technique to real-world systems. It is probably not possible to develop a general solution for estimating M_e, but it may be tractable to constrain M_e for a specific application at a specific scale of space and time.

We know that for steady states, the Dynamical Shannon entropy is zero, and information flow is also zero. The most trivial steady state for our application is the case where the $E = 0\ \mathrm{W\,m^{-2}}$ at all points in time. In this case there is no error residual, and it is clear that there the Shannon entropy of the residual error $S(E) = 0$ and all information flows to E are also zero. On the other hand, if the average value of E is zero across "slow" scales of time (e.g. 4+ h in this study), there may still be significant information flow at shorter timescales as any given timestep still shows dynamics. This information conservation framework is incapable of measuring *any* information flow associated with steady-state processes. For example, if there were a steady and unobserved leak of energy from the system via some unobserved storage flux, this would not appear in the Shannon entropy of the residual *S(E)* or in the information flows to the residual. As a result, this method is useful as a diagnostic to identify "fast" canceling errors in a timeseries, or for the attribution of "fast" random error, but it cannot tell us about systematic bias in the mean values (i.e. bias in the "slow" dynamics of the system). Dynamical information technique focuses on and depends upon the time-variance of the data, not on mean values of the data. When used in combination with other techniques that directly address bulk closure and bias, this information closure technique complements the other methods.

References

Araújo, A.C., Nobre, A.D., Kruijt, B., Elbers, J.A., Dallarosa, R., Stefani, P., Von Randow, C., Manzi, A.O., Culf, A.D., Gash, J.H.C., 2002. Comparative measurements of carbon dioxide fluxes from two nearby towers in a central Amazonian rainforest: the Manaus LBA site. J. Geophys. Res. Atmos. 107 (D20), 8090.

Avissar, R., Werth, D., 2005. Global hydroclimatological teleconnections resulting from tropical deforestation. J. Hydrometeorol. 6, 134–145.

Badiya Roy, S., Avissar, R., 2002. Impact of land use/land cover change on regional hydrometeorology in Amazonia. J. Geophys. Res. 107. http://dx.doi.org/10.1029/2000jd000266.

Baldocchi, D., Falge, E., Gu, L.H., Olson, R., Hollinger, D., Running, S., Anthoni, P., Bernhofer, C., Davis, K., Evans, R., Fuentes, J., Goldstein, A., Katul, G., Law, B., Lee, X.H., Malhi, Y., Meyers, T., Munger, W., Oechel, W., Paw, U.K.T., Pilegaard, K., Schmid, H.P., Valentini, R., Verma, S., Vesala, T., Wilson, K., Wofsy, S., 2001. FLUXNET: a new tool to study the temporal and spatial variability of ecosystem-scale carbon dioxide, water vapor, and energy flux densities. Bull. Am. Meteorol. Soc. 82, 2415–2434.

Baldocchi, D., 2008. Breathing of the terrestrial biosphere: lessons learned from a global network of carbon dioxide flux measurement systems. Aust. J. Bot. 56, 1–26. http://dx.doi.org/10.1071/BT07151.

Baldocchi, D., 2014. Measuring fluxes of trace gases and energy between ecosystems and the atmosphere–the state and future of the eddy covariance method. Glob. Change Biol. 20, 3600–3609.

Charuchittipan, D., Babel, W., Mauder, M., Leps, J.-P., Foken, T., 2014. Extension of the averaging time in eddy-covariance measurements and Its effect on the energy balance closure. Bound.-Layer Meteorol. 152, 303–327. http://dx.doi.org/10.1007/s10546-014-9922-6.

Cox, P.M., Betts, R.A., Jones, C.D., Spall, S.A., Totterdell, I.J., 2000. Acceleration of global warming due to carbon-cycle feedbacks in a coupled climate model. Nature 408, 184–187.

Fisher, R.A., Williams, M., Do Vale, R.L., Da Costa, A.L., Meir, P., 2006. Evidence from Amazonian forests is consistent with isohydric control of leaf water potential. Plant Cell Environ. 29, 151–165. http://dx.doi.org/10.1111/j.1365-3040.2005.01407.x.

Foken, T., Wimmer, F., Mauder, M., Thomas, C., Liebethal, C., 2006. Some aspects of the energy balance closure problem. Atmos. Chem. Phys. 6, 4395–4402.

Foken, T., Aubinet, M., Finnigan, J.J., Leclerc, M.Y., Mauder, M., Paw, U.K.T., 2011. Results of a panel discussion about the energy balance closure correction for trace gases. Bull. Am. Meteorol. Soc. 92, ES13–ES18. http://dx.doi.org/10.1175/2011BAMS3130.1.

Foken, T., 2008. The energy balance closure problem: an overview. Ecol. Appl. 18, 1351–1367. http://dx.doi.org/10.1890/06-0922.1.

Frank, J.M., Massman, W.J., Ewers, B.E., 2013. Underestimates of sensible heat flux due to vertical velocity measurement errors in non-orthogonal sonic anemometers. Agric. For. Meteorol. 171–172, 72–81. http://dx.doi.org/10.1016/j.agrformet.2012.11.005.

Franssen, H.J.H., Stöckli, R., Lehner, I., Rotenberg, E., Seneviratne, S.I., 2010. Energy balance closure of eddy-covariance data: a multisite analysis for European FLUXNET stations. Agric. For. Meteorol. 150, 1553–1567. http://dx.doi.org/10.1016/j.agrformet.2010.08.005.

Freire, L.S., Gerken, T., Ruiz-Plancarte, J., Wei, D., Fuentes, J.D., Katul, G.G., Dias, N.L., Acevedo, O.C., Chamecki, M., 2017. Turbulent mixing and removal of ozone within an Amazon rainforest canopy. J. Geophys. Res. Atmos. 122, 2791–2811. http://dx.doi.org/10.1002/2016JD026009.

Fuentes, J.D., Chamecki, M., Nascimento dos Santos, R.M., Von Randow, C., Stoy, P.C., Katul, G., Fitzjarrald, D., Manzi, A., Gerken, T., Trowbridge, A., Souza Freire, L., Ruiz-Plancarte, J., Furtunato Maia, J.M., Tóta, J., Dias, N., Fisch, G., Schumacher, C., Acevedo, O., Mercer, J.R., 2016. Linking meteorology, turbulence, and air chemistry in the Amazon rainforest. Bull. Am. Meteorol. Soc. 97, 2329–2342. http://dx.doi.org/10.1175/BAMS-D-15-00152.1.

Gatti, L.V., Gloor, M., Miller, J.B., Doughty, C.E., Malhi, Y., Domingues, L.G., Basso, L.S., Martinewski, A., Correia, C.S.C., Borges, V.F., 2014. Drought sensitivity of Amazonian carbon balance revealed by atmospheric measurements. Nature 506, 76–80.

Goodwell, A., Kumar, P., 2015. Information theoretic measures to infer feedback dynamics in coupled logistic networks. Entropy 17, 7468–7492.

Gu, L., Massman, W.J., Leuning, R., Pallardy, S.G., Meyers, T., Hanson, P.J., Riggs, J.S., Hosman, K.P., Yang, B., 2012. The fundamental equation of eddy covariance and its application in flux measurements. Agric. For. Meteorol. 152, 135–148.

Haverd, V., Cuntz, M., Leuning, R., Keith, H., 2007. Air and biomass heat storage fluxes in a forest canopy: calculation within a soil vegetation atmosphere transfer model. Agric. For. Meteorol. 147, 125–139. http://dx.doi.org/10.1016/j.agrformet.2007.07.006.

Hodnett, M.G., Da Silva, L.P., Da Rocha, H.R., Senna, R.C., 1995. Seasonal soil water storage changes beneath central Amazonian rainforest and pasture. J. Hydrol. 170, 233–254.

Huete, A.R., Didan, K., Shimabukuro, Y.E., Ratana, P., Saleska, S.R., Hutyra, L.R., Yang, W., Nemani, R.R., Myneni, R., 2006. Amazon rainforests green-up with sunlight in dry season. Geophys. Res. Lett. 33, L06405. http://dx.doi.org/10.1029/2005GL025583.

Jardine, A.B., Jardine, K.J., Fuentes, J.D., Martin, S.T., Martins, G., Durgante, F., Carneiro, V., Higuchi, N., Manzi, A.O., Chambers, J.Q., 2015. Highly reactive light-dependent monoterpenes in the Amazon. Geophys. Res. Lett. 42, 1576–1583. http://dx.doi.org/10.1002/2014GL062573.

Jung, M., Reichstein, M., Ciais, P., Seneviratne, S.I., Sheffield, J., Goulden, M.L., Bonan, G., Cescatti, A., Chen, J., de Jeu, R., Dolman, A.J., Eugster, W., Gerten, D., Gianelle, D., Gobron, N., Heinke, J., Kimball, J., Law, B.E., Montagnani, L., Mu, Q., Mueller, B., Oleson, K., Papale, D., Richardson, A.D., Roupsard, O., Running, S., Tomelleri, E., Viovy, N., Weber, U., Williams, C., Wood, E., Zaehle, S., Zhang, K., 2010. Recent decline in the global land evapotranspiration trend due to limited moisture supply. Nature 467, 951–954. http://dx.doi.org/10.1038/nature09396.

Kang, M., Ruddell, B.L., Cho, C., Chun, J., Kim, J., 2017. Identifying CO_2 advection on a hill slope using information flow. Agric. For. Meteorol. 232, 265–278.

Kim, D.-H., Sexton, J.O., Townshend, J.R., 2015. Accelerated deforestation in the humid tropics from the 1990 to the 2000. Geophys. Res. Lett. 42, 3495–3501. http://dx.doi.org/10.1002/2014GL062777.

Klein, T., 2014. The variability of stomatal sensitivity to leaf water potential across tree species indicates a continuum between isohydric and anisohydric behaviours. Funct. Ecol. 28, 1313–1320. http://dx.doi.org/10.1111/1365-2435.12289.

Kochendorfer, J., Meyers, T.P., Frank, J., Massman, W.J., Heuer, M.W., 2012. How well can we measure the vertical wind speed? Implications for fluxes of energy and mass. Bound.-Layer Meteorol. 145, 383–398. http://dx.doi.org/10.1007/s10546-012-9738-1.

Konings, A.G., Gentine, P., 2016. Global variations in ecosystem-scale isohydricity. Glob. Change Biol. http://dx.doi.org/10.1111/gcb.13389.

Kracher, D., Mengelkamp, H.-T., Foken, T., 2009. The residual of the energy balance closure and its influence on the results of three SVAT models. Meteorol. Zeitschrift 18, 647–661.

Kruijt, B., Malhi, Y., Lloyd, J., Norbre, A.D., Miranda, A.C., Pereira, M.G.P., Culf, A., Grace, J., 2000. Turbulence statistics above and within two Amazon rain forest canopies. Bound.-Layer Meteorol. 94, 297–331.

Kruijt, B., Elbers, J.A., Von Randow, C., Araujo, A.C., Oliveira, P.J., Culf, A., Manzi, A.O., Nobre, A.D., Kabat, P., Moors, E.J., 2004. The robustness of eddy correlation fluxes for Amazon rain forest conditions. Ecol. Appl. 14, 101–113.

Kumagai, T., Porporato, A., 2012. Strategies of a Bornean tropical rainforest water use as a function of rainfall regime: isohydric or anisohydric? Plant Cell Environ. 35, 61–71. http://dx.doi.org/10.1111/j.1365-3040.2011.02428.x.

Leuning, R., van Gorsel, E., Massman, W.J., Isaac, P.R., 2012. Reflections on the surface energy imbalance problem. Agric. For. Meteorol. 156, 65–74. http://dx.doi.org/10.1016/j.agrformet.2011.12.002.

Levine, N.M., Zhang, K., Longo, M., Baccini, A., Phillips, O.L., Lewis, S.L., Alvarez-Dávila, E., Segalin de Andrade, A.C., Brienen, R.J.W., Erwin, T.L., Feldpausch, T.R., Monteagudo Mendoza, A.L., Nuñez Vargas, P., Prieto, A., Silva-Espejo, J.E., Malhi, Y., Moorcroft, P.R., 2016. Ecosystem heterogeneity determines the ecological resilience

of the Amazon to climate change. Proc. Natl. Acad. Sci. 113, 793–797. http://dx.doi.org/10.1073/pnas.1511344112.

Malhi, Y., Nobre, A.D., Grace, J., Kruijt, B., Pereira, M.G.P., Culf, A., Scott, S., 1998. Carbon dioxide transfer over a central Amazonian rain forest. J. Geophys. Res. 103, 31593–31612.

Malhi, Y., Pegorano, E., Nobre, A.D., Pereira, M.G.P., Grace, J., Culf, A.D., Clement, R., 2002. Energy and water dynamics of a central Amazonian rain forest. J. Geophys. Res. 107, 8061. http://dx.doi.org/10.1029/2001JD000623.

Mallick, K., Trebs, I., Giustarini, L., Schlerf, M., Drewry, D., Hoffmann, L., von Randow, C., Kruijt, B., Saleska, S., Ehleringer, J.R., 2016. Canopy-scale biophysical controls on transpiration and evaporation in the Amazon Basin. Hydrol. Earth Syst. Sci. 20, 4237–4264. http://dx.doi.org/10.5194/hess-20-4237-2016.

Marques Filho, A.O., de Dallarosa, R.G., Pachêco, V.B., 2005. Radiaêço solar e distribuiêço vertical de ãrea foliar em floresta–Reserva Biológica do Cuieiras–ZF2, Manaus. Acta Amaz. 35, 427–436.

Martin, S.T., Artaxo, P., Machado, L., Manzi, A.O., Souza, R.A.F., Schumacher, C., Wang, J., Biscaro, T., Brito, J., Calheiros, A., 2016. The Green Ocean Amazon experiment (GoAmazon2014/5) observes pollution affecting gases, aerosols, clouds, and rainfall over the rain forest. Bull. Am. Meteorol. Soc.. http://dx.doi.org/10.1175/bams-d-15-00221.1. early online release.

Massman, W., Clement, R., 2004. Uncertainty in eddy covariance flux estimates resulting from spectral attenuation. Handbook of Micrometeorology. Springerpp. 67–99.

Massman, W.J., Lee, X., 2002. Eddy covariance flux corrections and uncertainties in long-term studies of carbon and energy exchanges. Agric. For. Meteorol. 113, 121–144.

Mauder, M., Foken, T., 2004. Documentation and Instruction Manual of the Eddy Covariance Software Package TK2. Univ., Abt. Mikrometeorologie.

Mauder, M., Desjardins, R.L., MacPherson, I., 2007. Scale analysis of airborne flux measurements over heterogeneous terrain in a boreal ecosystem. J. Geophys. Res. 112, 1–13. http://dx.doi.org/10.1029/2006JD008133.

Mauder, M., Desjardins, R.L., Pattey, E., Worth, D., 2010. An attempt to close the daytime surface energy balance using spatially-averaged flux measurements. Bound.-Layer Meteorol. 136, 175–191.

Medvigy, D., Walko, R.L., Otte, M.J., Avissar, R., 2013. Simulated changes in northwest US climate in response to Amazon deforestation. J. Clim. 26, 9115–9136.

Moncrieff, J., Clement, R., Finnigan, J., Meyers, T., 2005. Averaging, detrending, and filtering of eddy covariance time series. In: Lee, X., Massman, W., Law, B.E. (Eds.), Handbook of Micrometeorology. Springer, pp. 7–31.

Morton, D.C., Nagol, J., Carabajal, C.C., Rosette, J., Palace, M., Cook, B.D., Vermote, E.F., Harding, D.J., North, P.R.J., 2014. Amazon forests maintain consistent canopy structure and greenness during the dry season. Nature 506, 221–224.

Novick, K.A., Ficklin, D.L., Stoy, P.C., Williams, C.A., Bohrer, G., Oishi, A.C., Papuga, S.A., Blanken, P.D., Noormets, A., Sulman, B.N., Scott, R.L., Wang, L., Phillips, R.P., 2016. The increasing importance of atmospheric demand for ecosystem water and carbon fluxes. Nat. Clim. Change 6, 1023–1027.

Panin, G.N., Bernhofer, C., 2008. Parametrization of turbulent fluxes over inhomogeneous landscapes. Izv. Atmos. Ocean. Phys. 44, 701–716. http://dx.doi.org/10.1134/S0001433808060030.

Paninski, L., 2003. Estimation of entropy and mutual information. Neural Comput. 15, 1191–1253.

Papale, D., Reichstein, M., Aubinet, M., Canfora, E., Bernhofer, C., Kutsch, W., Longdoz, B., Rambal, S., Valentini, R., Vesala, T., Yakir, D., 2006. Towards a standardized processing of net ecosystem exchange measured with eddy covariance technique: algorithms and uncertainty estimation. Biogeosciences 3, 571–583.

Pavlick, R., Drewry, D.T., Bohn, K., Reu, B., Kleidon, A., 2013. The Jena Diversity-Dynamic Global Vegetation Model (JeDi-DGVM): a diverse approach to representing terrestrial biogeography and biogeochemistry based on plant functional trade-offs. Biogeosciences 10, 4137–4177.

Richardson, A.D., Hollinger, D.Y., Burba, G.G., Davis, K.J., Flanagan, L.B., Katul, G.G., Munger, J.W., Ricciuto, D.M., Stoy, P.C., Suyker, A.E., Verma, S.B., Wofsy, S.C., 2006. A multi-site analysis of random error in tower-based measurements of carbon and energy fluxes. Agric. For. Meteorol. 136, 1–18.

Ruddell, B.L., Kumar, P., 2009a. Ecohydrologic process networks: 1. Identification. Water Resour. Res. 45, 1–22. http://dx.doi.org/10.1029/2008WR007279.

Ruddell, B.L., Kumar, P., 2009b. Ecohydrologic process networks: 2. Analysis and characterization. Water Resour. Res. 45, 1–14. http://dx.doi.org/10.1029/2008WR007280.

Ruddell, B.L., Brunsell, N.A., Stoy, P.C., 2013. Applying information theory in the geosciences to quantify process uncertainty, feedback, scale. Eos Trans. Am. Geophys. Union 94, 56.

Ruddell, B.L., Yu, R., Kang, M., Childers, D.L., 2015. Seasonally varied controls of climate and phenophase on terrestrial carbon dynamics: modeling eco-climate system state using Dynamical Process Networks. Landsc. Ecol. 31, 165–180. http://dx.doi.org/10.1007/s10980-015-0253-x.

Saleska, S.R., Didan, K., Huete, A.R., Da Rocha, H.R., 2007. Amazon forests green-up during 2005 drought. Science (80-.) 318, 612.

Saleska, S.R., Wu, J., Guan, K., Araujo, A.C., Huete, A., Nobre, A.D., Restrepo-Coupe, N., 2016. Dry-season greening of Amazon forests. Nature 531, E4–E5.

Santos, D.M., Acevedo, O.C., Chamecki, M., Fuentes, J.D., Gerken, T., Stoy, P.C., 2016. Temporal scales of the nocturnal flow within and above a forest canopy in Amazonia. Bound.-Layer Meteorol. 1–26. http://dx.doi.org/10.1007/s10546-016-0158-5.

Stoy, P.C., Richardson, A.D., Baldocchi, D.D., Katul, G.G., Stanovick, J., Mahecha, M.D., Reichstein, M., Detto, M., Law, B.E., Wohlfahrt, G., Arriga, N., Campos, J., McCaughey, J.H., Montagnani, L., Paw, U.K.T., Sevanto, S., Williams, M., 2009. Biosphere-atmosphere exchange of CO_2 in relation to climate: a cross-biome analysis across multiple time scales. Biogeosciences 6, 2297–2312.

Stoy, P., Mauder, M., Foken, T., Marcolla, B., Boegh, E., Ibrom, A., Arain, M.A., Arneth, A., Aurela, M., Bernhofer, C., Cescatti, A., Dellwik, E., Duce, P., Gianelle, D., van Gorsel, E., Kiely, G., Knohl, A., Margolis, H., McCaughey, H., Merbold, L., Montagnani, L., Papale, D., Reichstein, M., Saunders, M., Serrano-Ortiz, P., Sottocornola, M., Spano, D., Vaccari, F., Varlagin, A., 2013. A data-driven analysis of energy balance closure across FLUXNET research sites: the role of landscape scale heterogeneity. Agric. For. Meteorol. 171, 137–152.

Stull, R.B., 1988. An Introduction to Boundary Layer Meteorology. Springer Science & Business Media.

Sturtevant, C., Ruddell, B.L., Knox, S.H., Verfaillie, J., Matthes, J.H., Oikawa, P.Y., Baldocchi, D., 2016. Identifying scale-emergent, nonlinear, asynchronous processes of wetland methane exchange. J. Geophys. Res. Biogeosci.

Sulman, B.N., Roman, D.T., Yi, K., Wang, L., Phillips, R.P., Novick, K.A., 2016. High atmospheric demand for water can limit forest carbon uptake and transpiration as severely as dry soil. Geophys. Res. Lett. 43, 9686–9695. http://dx.doi.org/10.1002/2016GL069416.

Sultan, B., Janicot, S., 2000. Abrupt shift of the ITCZ over West Africa and intra-seasonal variability. Geophys. Res. Lett. 27, 3353–3356.

Tóta, J., Fitzjarrald, D.R., da Silva Dias, M.A.F., 2012. Amazon rainforest exchange of carbon and subcanopy air flow: manaus LBA site—a complex terrain condition. Sci. World J. 165067. http://dx.doi.org/10.1100/2012/165067.

Twine, T.E., Kustas, W.P., Norman, J.M., Cook, D.R., Houser, P.R., Meyers, T.P., Prueger, J.H., Starks, P.J., Wesely, M.L., 2000. Correcting eddy-covariance flux underestimates over a grassland. Agric. For. Meteorol. 103, 279–300.

Voigt, A., Bony, S., Dufresne, J., Stevens, B., 2014. The radiative impact of clouds on the shift of the intertropical convergence zone. Geophys. Res. Lett. 41, 4308–4315.

Webb, E.K., Pearman, G.I., Leuning, R., 1980. Correction of flux measurements for density effects due to heat and water vapour transfer. Q. J. R. Meteorol. Soc. 106, 85–100.

Weijs, S.V., 2011. Information Theory for Risk-Based Water System Operation. Delft University of Technology, TU Delft.

Williams, C.A., Reichstein, M., Buchmann, N., Baldocchi, D., Beer, C., Schwalm, C., Wohlfahrt, G., Hasler, N., Bernhofer, C., Foken, T., Papale, D., Schymanski, S., Schaefer, K., 2012. Climate and vegetation controls on the surface water balance: synthesis of evapotranspiration measured across a global network of flux towers. Water Resour. Res. 48, W06523. http://dx.doi.org/10.1029/2011WR011586.

Wilson, K., Goldstein, A., Falge, E., Aubinet, M., Baldocchi, D., Berbigier, P., Bernhofer, C., Ceulemans, R., Dolman, H., Field, C., Grelle, A., Ibrom, A., Law, B.E., Kowalski, A., Meyers, T., Moncrieff, J., Monson, R., Oechel, W., Tenhunen, J., Valentini, R., Verma, S., 2002. Energy balance closure at FLUXNET sites. Agric. For. Meteorol. 113, 223–243.

Zeng, N., Yoon, J.-H., Marengo, J.A., Subramaniam, A., Nobre, C.A., Mariotti, A., Neelin, J.D., 2008. Causes and impacts of the 2005 Amazon drought. Environ. Res. Lett. 3, 14002.

da Rocha, H.R., Goulden, M.L., Miller, S.D., Menton, M.C., Pinto, L.D.V.O., de Freitas, H.C., de Silva Figueira, A.M., 2004. Seasonality of wtaer and heat fluxes over a tropical forest in eastern Amazonia. Ecol. Appl. 14, 22–32. http://dx.doi.org/10.1890/02-6001.

da Rocha, H.R., Manzi, A.O., Cabral, O.M., Miller, S.D., Goulden, M.L., Saleska, S.R., R.-Coupe, N., Wofsy, S.C., Borma, L.S., Artaxo, P., Vourlitis, G., Nogueira, J.S., Cardoso, F.L., Nobre, A.D., Kruijt, B., Freitas, H.C., von Randow, C., Aguiar, R.G., Maia, J.F., 2009. Patterns of water and heat flux across a biome gradient from tropical forest to savanna in Brazil. J. Geophys. Res. Biogeosci. 114, G00B12. http://dx.doi.org/10.1029/2007JG000640.